

iSeg: Interactive 3D Segmentation via Interactive Attention

ITAI LANG*, University of Chicago, USA

FEI XU*, University of Chicago, USA

DALE DECATUR, University of Chicago, USA

SUDARSHAN BABU, Toyota Technological Institute at Chicago, USA

RANA HANOCKA, University of Chicago, USA

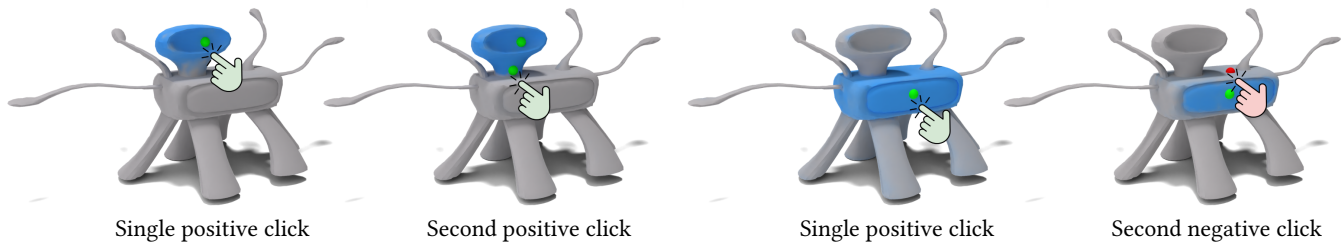


Fig. 1. iSeg computes customized fine-grained segmentations on shapes interactively specified by user clicks. The clicks, denoted by a green or a red dot, indicate whether to include or exclude regions, respectively. Our method is capable of segmenting regions that are not accurately specified by text.

We present iSeg, a new interactive technique for segmenting 3D shapes. Previous works have focused mainly on leveraging pre-trained 2D foundation models for 3D segmentation based on text. However, text may be insufficient for accurately describing fine-grained spatial segmentations. Moreover, achieving a consistent 3D segmentation using a 2D model is challenging since occluded areas of the same semantic region may not be visible together from any 2D view. Thus, we design a segmentation method conditioned on fine user clicks, which operates entirely in 3D. Our system accepts user clicks directly on the shape’s surface, indicating the inclusion or exclusion of regions from the desired shape partition. To accommodate various click settings, we propose a novel interactive attention module capable of processing different numbers and types of clicks, enabling the training of a single unified interactive segmentation model. We apply iSeg to a myriad of shapes from different domains, demonstrating its versatility and faithfulness to the user’s specifications. Our project page is at <https://threedle.github.io/iSeg/>.

CCS Concepts: • **Computing methodologies** → **Shape representations**; *Image segmentation*; • **Human-centered computing** → **Interactive systems and tools**.

Additional Key Words and Phrases: 3D mesh representation, Interactive segmentation, Differentiable rendering, Deep Learning, Knowledge distillation

1 INTRODUCTION

Interactive 3D segmentation is the ability to select fine-grained segments from a 3D shape that adhere to user inputs such as clicks. By contrast, traditional segmentation techniques do not utilize user inputs and instead rely on geometric features to delineate semantic parts [Cornea et al. 2007; Dey and Zhao 2004; Hoffman and Richards 1984; Lien and Amato 2007; Shamir 2008; Zheng et al. 2015].

In recent years, data-driven techniques have accelerated the 3D segmentation research by leveraging fully annotated 3D data [Chen

et al. 2019; Deng et al. 2020; Hanocka et al. 2019; Hu et al. 2022; Lahav and Tal 2020; Milano et al. 2020; Milletari et al. 2016; Qi et al. 2017; Sharp et al. 2022; Sun et al. 2021; Yi et al. 2017; Zhu et al. 2020]. However, the reliance on a dataset and the scarcity of large-scale 3D datasets limits the network to a specific shape domain with a predefined set of parts.

Recent 3D segmentation techniques have circumvented the dependency on 3D data and pre-determined part definition by utilizing pre-trained 2D foundation models to learn semantic co-segmentation [Ye et al. 2023] or text-driven segmentation [Abdelreheem et al. 2023a,b; Decatur et al. 2023a,b; Ha and Song 2022; Kobayashi et al. 2022]. However, text may not be able to accurately describe all fine-grained segmentations, such as the fourth leg of an octopus or a region corresponding to a particular point on the shape.

In this work, we present *iSeg*, a new data-driven interactive technique for 3D shape segmentation that generates tailored partitions of the shape according to user clicks. Given a shape represented as a triangular mesh, the user selects points on the mesh interactively to indicate a desired segmentation and iSeg predicts a region over the mesh surface that adheres to the clicked points. Our interactive interface can utilize positive and negative clicks, enabling additions and exclusions of areas from the segmented region, respectively (see for example Fig. 1).

We harness the power of a pretrained 2D foundation segmentation model [Kirillov et al. 2023] and distill its knowledge to 3D. However, segmenting a meaningful 3D region using a 2D model is very challenging, since occluded shape regions cannot be seen together from a single 2D view. Accordingly, we design an interactive segmentation system that operates *entirely in 3D*, where the user clicks and the inferred corresponding region are done over the shape surface *directly*, ensuring 3D consistency *by construction*. During training only, we project the 3D user clicks and the predicted segmentation to multiple 2D views to enjoy supervision from the powerful pretrained foundation model [Kirillov et al. 2023].

*Equal contribution

Authors’ addresses: Itai Lang, University of Chicago, USA, itailang@uchicago.edu; Fei Xu*, University of Chicago, USA, feixu@uchicago.edu; Dale Decatur, University of Chicago, USA, ddecatur@uchicago.edu; Sudarshan Babu, Toyota Technological Institute at Chicago, USA, sudarshan@ttic.edu; Rana Hanocka, University of Chicago, USA, ranahanocka@uchicago.edu.

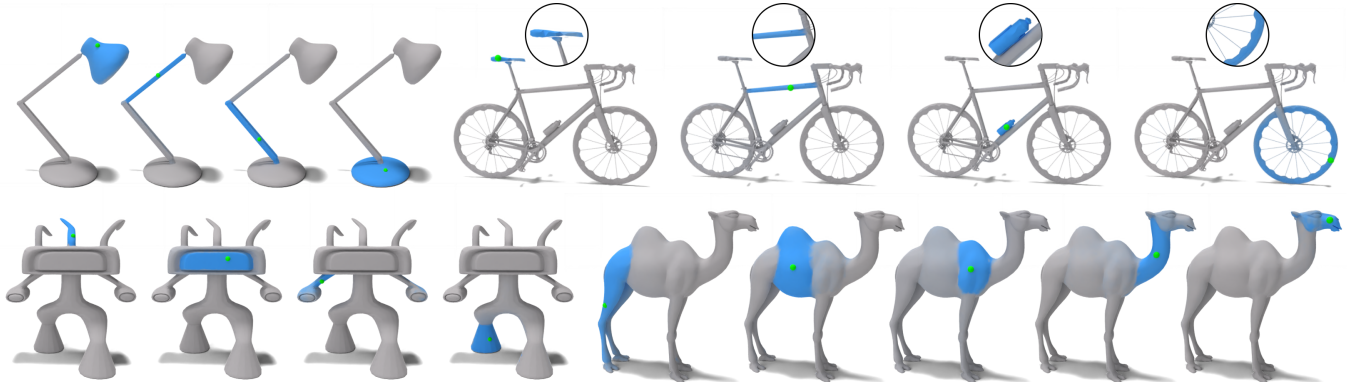


Fig. 2. **Fine-grained segmentation from a single positive click.** iSeg is capable of generating granular segmentations (visualized in blue) given a single click as input (depicted with a green dot). Our method is highly flexible and can select parts that vary in size, geometry, and semantic meaning.

For interactivity, we want our system to accommodate different user inputs, meaning, point clicks that can vary in number and type. Instead of training a separate segmentation model for each user click configuration, we propose a novel interactive attention mechanism, which learns the representation of positive and negative clicks and computes their interaction with the other points of the mesh. This attention layer consolidates variable-size guidance into a fixed-size representation, resulting in a unified flexible segmentation model capable of predicting shape regions for various click settings.

In summary, this paper presents iSeg, an interactive method for selecting customized fine-grained regions on a 3D shape. We distill inconsistent feature embeddings of a 2D foundation model into a coherent feature field over the mesh surface and decode it along with user inputs to segment the mesh on the fly. Our interactive attention mechanism handles a variable number of user clicks that can signify both the inclusion and exclusion of regions. We showcase the effectiveness of iSeg on a variety of meshes from different domains, including humanoids, animals, and man-made objects, and show its flexibility for various segmentation specifications.

2 RELATED WORK

Non-interactive 3D Segmentation. A large body of research has been focused on 3D segmentation using annotated datasets [Armeni et al. 2017; Hanocka et al. 2019; Hu et al. 2022; Lahav and Tal 2020; Milano et al. 2020; Sharp et al. 2022; Yi et al. 2017]. Such models demonstrate impressive performance at the cost of being restricted to the domain of the training data and the set of manually defined semantic labels. A partial solution to this limitation is utilizing unlabeled data, where common semantic elements are discovered by unsupervised learning [Chen et al. 2019; Deng et al. 2020; Hong et al. 2022; Sun et al. 2021; Zhu et al. 2020]. Still, the segmentation is confined to the learned parts and is not easy to alter.

In contrast, our segmentation approach is highly versatile and flexible. It is applied to various shapes from different domains. Our model is trained without any segment labels, and instead, it is optimized to the shape at hand to discover its unique partitions. Moreover, iSeg is interactive – its segmentation result can be updated simply with an intuitive user-click interface.

Lifting 2D foundation models to 3D. The emergence of powerful 2D foundation models with a broad semantic understanding has propelled a surge of interest in distilling their knowledge and lifting it to a 3D representation [Abdelreheem et al. 2023a,b; Chen et al. 2023a; Decatur et al. 2023a,b; Goel et al. 2023b; Kerr et al. 2023; Kobayashi et al. 2022; Kundu et al. 2020; Ye et al. 2023; Zhang et al. 2022]. Notably, [Kobayashi et al. 2022] and [Kerr et al. 2023] augmented the neural radiance scene representation (NeRF) [Mildenhall et al. 2020] with a volumetric feature field. This approach enabled text-driven segmentation of objects within the scene, alleviating the need for a training dataset.

Similarly, we also lift the features of a 2D foundation model [Kirillov et al. 2023] into 3D. However, our method differs from previous work in several aspects. First, instead of using the implicit NeRF representation [Kerr et al. 2023; Kobayashi et al. 2022], our model operates directly on explicit 3D meshes, making it readily adaptable to 3D modeling workflows. Second, instead of learning an entire 3D feature volume, our mesh feature field lives only on the shape’s surface, simplifying the distillation process and making it more tractable. Third, rather than decoding the feature field with a simple correlation with the embedding of the semantic prompt, we learn a dedicated decoder in 3D to better exploit the semantic information embodied within our mesh feature field.

Interactive 3D Segmentation. Traditional interactive techniques have utilized heuristic smoothness priors and formulated the problem with a graph cut optimization objective [Boykov and Jolly 2001; Levin et al. 2007; Rother et al. 2004; Sormann et al. 2006]. More recently, several learning-based methods have been proposed for interactive segmentation [Goel et al. 2023a; Kontogianni et al. 2023; Yue et al. 2023]. For example, [Kontogianni et al. 2023] segmented 3D point clouds based on user clicks. Unlike our work, they constructed a dataset for training their model, which limited its utility to parsing objects from a point cloud scene.

Very recently, [Kirillov et al. 2023] presented a foundation model for 2D interactive segmentation termed SAM, which triggered a line of follow-up works aiming at harnessing SAM’s impressive capabilities to the 3D domain [Cen et al. 2023; Chen et al. 2023b; Yang et al. 2023; Zhang et al. 2023]. One approach is to segment

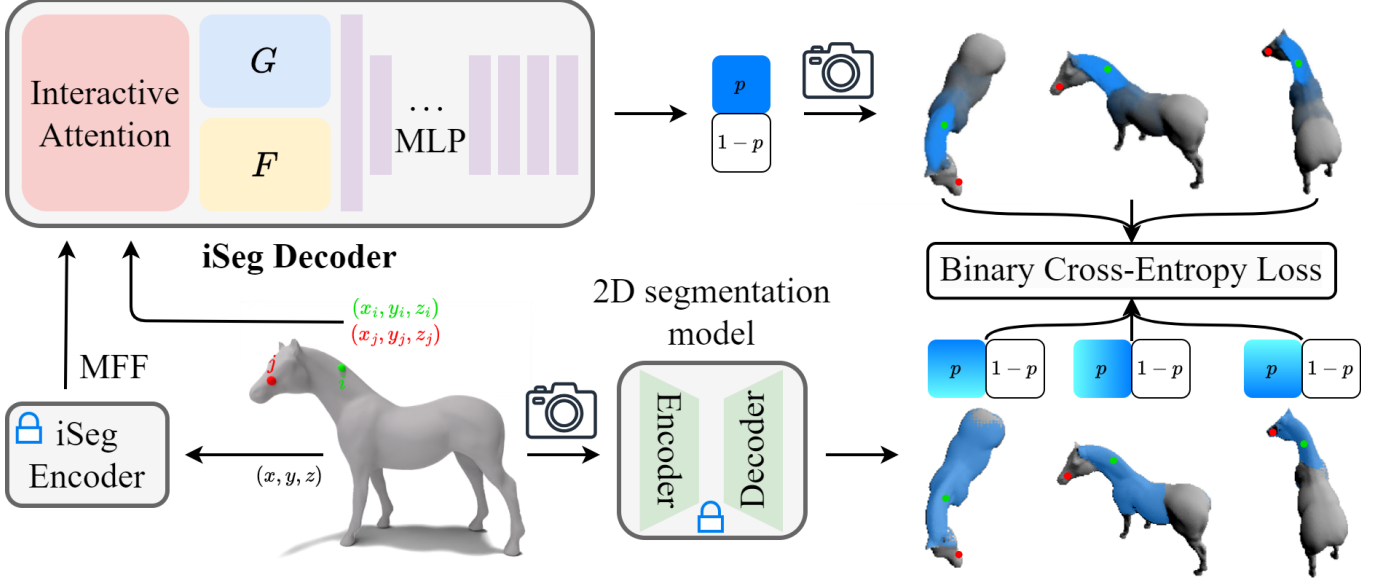


Fig. 3. **Training of iSeg decoder.** Our decoder takes the Mesh Feature Field (MFF) from iSeg encoder, along with the user input clicks, and generates a 3D segmentation map visualized in blue. We leverage a pre-trained 2D segmentation model [Kirillov et al. 2023] to supervise our training with 2D segmentation masks using rendered images of the shape and the 2D projection of the 3D clicks. Although iSeg is trained using noisy and inconsistent 2D segmentations, it is view-consistent by construction.

2D projections of the 3D data and fuse them in 3D. However, such an approach requires high user guidance, as the segmentation is performed in 2D, and the user’s input is required for different views.

Another approach taken by [Chen et al. 2023b] is to lift SAM’s features to a NeRF representation and use SAM’s decoder to obtain the segmentation masks. As in the first approach, applying the segmentation in 2D limits the method’s capabilities, since it cannot segment together occluded regions in 3D that are not visible concurrently in any 2D view. In contrast to existing works, our model and the user clicks are applied directly in 3D, simplifying the segmentation process and enabling the native segmentation of meaningful regions in 3D (as demonstrated in Fig. 5).

3 METHOD

Given a 3D shape depicted as a mesh \mathcal{M} with vertices $V = \{v_i\}_{i=1}^n$, $v_i = (x_i, y_i, z_i) \in \mathbb{R}^3$, and a set of selected vertices by the user representing positive or negative clicks, our goal is to predict the per-vertex probability $P = \{p_i\}_{i=1}^n$, $p_i \in [0, 1]$ of belonging to a region adhering to the user inputs. Our system offers an interactive user interface, such that the number of clicks and their type can be varied and the segmented region of the shape is updated accordingly.

We tackle the problem by proposing an interactive segmentation technique consisting of two parts: an encoder that maps vertex coordinates to a deep semantic vector, denoted as Mesh Feature Field (MFF), and a decoder that takes the MFF and the user clicks and predicts the corresponding mesh segment. The decoder contains an interactive attention layer supporting a variable number of clicks, which can be positive or negative, to increase or decrease the segmented region. Figure 3 presents an overview of the method.

3.1 Mesh Feature Field

The Mesh Feature Field (MFF) is a function $\phi: \mathbb{R}^3 \rightarrow \mathbb{R}^d$ that embeds each mesh vertex into a deep feature vector $\phi(v_i) = f_i$, where d is the feature dimension. The MFF distills the semantic information from a pretrained 2D foundation model for image segmentation [Kirillov et al. 2023] and facilitates a 3D consistent feature representation for interactive segmentation of the mesh. To train the MFF, we render the high-dimensional vertex attributes differentially and obtain the 2D projected features:

$$I_f^\theta = \mathcal{R}(\mathcal{M}, f, \theta) \in \mathbb{R}^{w \times h \times d}, \quad (1)$$

where \mathcal{R} is a differentiable renderer, θ is the viewing direction, and $w \times h$ are the spatial dimensions of the rasterized image.

The MFF is implemented as a multi-layer perceptron network, regarded as iSeg Encoder. To supervise its training, we render the mesh into a color image I_c^θ and pass it through the encoder E_{2D} of the 2D foundation model [Kirillov et al. 2023] to obtain a reference feature map:

$$I_e^\theta = E_{2D}(I_c^\theta) \in \mathbb{R}^{w \times h \times d}. \quad (2)$$

This process is repeated for multiple random viewing angles Θ , and our encoder is trained to minimize the discrepancy between the rendered MFF and the reference 2D features:

$$\mathcal{L}_{enc} = \frac{1}{|\Theta|} \sum_{\theta \in \Theta} \|I_f^\theta - I_e^\theta\|^2. \quad (3)$$

The 2D model operates on each image separately and might produce inconsistent features for different views of shape. In contrast, our MFF is defined in 3D and is view-consistent by construction. It consolidates the information from the multiple views and lifts

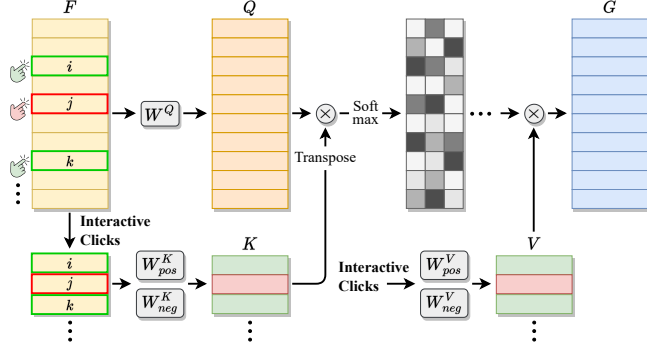


Fig. 4. **Interactive Attention.** Our interactive attention layer can handle a variable number of user clicks. The clicks may be positive or negative to indicate region inclusion or exclusion, respectively.

the 2D embeddings to a coherent field over the mesh surface. Additionally, we emphasize that the MFF is optimized independently of the user inputs. This is a key consideration in our method, resulting in a condition-agnostic representation, describing inherent semantic properties of the mesh. We validate this design choice with an ablation experiment demonstrated in Fig. 14 and explained in the supplementary. The MFF is optimized until convergence and then utilized together with the user click prompts to compute the interactive mesh partition.

3.2 Interactive Attention Layer

The interactive attention layer is part of the decoding component of our system (Fig. 3). Its structure is illustrated in Fig. 4. The layer computes the interaction between the user input clicks and the mesh vertices, accommodating variable numbers and types of clicks, positive and negative. This key element in our method enables a unified decoder architecture supporting various user click settings.

Our interactive attention extends the scaled dot-product attention mechanism [Vaswani et al. 2017]. We denote the encoded mesh features as $F \in \mathbb{R}^{n \times d}$. The features of the positively and negatively clicked vertices are marked as $F_{pos} \in \mathbb{R}^{n_{pos} \times d}$ and $F_{neg} \in \mathbb{R}^{n_{neg} \times d}$, respectively, where n_{pos} and n_{neg} are the number of clicks of each type. The interactive attention layer projects the mesh features to Queries and the features of the clicked points to Keys and Values:

$$\begin{aligned} Q &= FW^Q \in \mathbb{R}^{n \times d} \\ K_{\{pos,neg\}} &= F_{\{pos,neg\}} W_{\{pos,neg\}}^K \in \mathbb{R}^{n_{\{pos,neg\}} \times d} \\ V_{\{pos,neg\}} &= F_{\{pos,neg\}} W_{\{pos,neg\}}^V \in \mathbb{R}^{n_{\{pos,neg\}} \times d}, \end{aligned} \quad (4)$$

where $W^Q, W_{\{pos,neg\}}^K, W_{\{pos,neg\}}^V \in \mathbb{R}^{d \times d}$ are learnable weight matrices. Then, the mesh vertices are attended to the user clicks to obtain the conditioned mesh features:

$$G = \text{softmax} \left(\frac{QK^T}{\sqrt{d}} \right) V \in \mathbb{R}^{n \times d}, \quad (5)$$

where $K, V \in \mathbb{R}^{(n_{pos}+n_{neg}) \times d}$ are the concatenation of K_{pos}, K_{neg} and V_{pos}, V_{neg} , respectively.

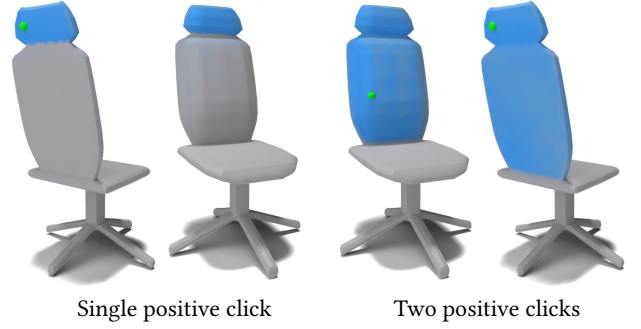


Fig. 5. **Native 3D segmentation.** iSeg segments parts in a 3D-consistent manner, regardless of whether the surface is occluded from the point click. A point is selected on the back of the chair (left), which is not visible from the front view. Still, our method delineates the occluded surface even though the 2D training data cannot contain this information. Furthermore, we may input two point clicks occluded from each other, one on the back of the chair and one on the front (right). These points cannot be simultaneously input to any 2D decoder, as they are not visible concurrently from any single viewpoint. Nonetheless, iSeg faithfully segments the whole backrest part.

Our attention mechanism condenses variable interactive user inputs into a fixed-length output. It learns the representation of positive and negative clicks, correlates the mesh vertices with them, and yields updated vertex features to enable the on-the-fly segmentation of the shape. Another benefit of our attention layer is that it is permutation invariant w.r.t. to the user clicks. In other words, it is independent of the sequential order of the point clicks and consistent in their joint influence on the shape partition. Moreover, the attention’s output G is permutation equivariant w.r.t. to vertex order in F , a desired property for the mesh data structure.

3.3 Segmentation Prediction

The output of our model is a segmentation of the mesh that adheres to the user clicks, represented as the per-vertex probability of belonging to the desired region. To do so, we learn to decode the a posteriori condition dependent vertex features $g_i = [G]_i$ and the a priori inherent embedding $f_i = [F]_i$ into the partition probability:

$$p_i = \psi(f_i, g_i) \in [0, 1]. \quad (6)$$

ψ is implemented as a multi-layer perceptron network, where f_i and g_i are concatenated along the feature dimension at the network’s input. The remaining question is – how to supervise the training of such an obscure and ill-defined problem?

Similar to our encoder’s training, we translate the problem to the 2D domain and harness the power of the 2D foundation model [Kirillov et al. 2023] for our 3D decoder learning (Fig. 3). We project the mesh probability map with a differentiable rasterizer to a probability image $I_p^{\theta'} = \mathcal{R}(\mathcal{M}, p, \theta') \in [0, 1]^{w' \times h' \times 2}$, where θ' is the viewing angle, and the image channels represent the segment and background probabilities. Then, we project the 3D clicks to their corresponding 2D pixels and use them as prompts to segment the rendered color mesh image with the 2D segmentation model, resulting in the supervising probability mask $I_m^{\theta'} \in \{0, 1\}^{w' \times h' \times 2}$. We randomize the viewing direction θ' and train our decoder subject

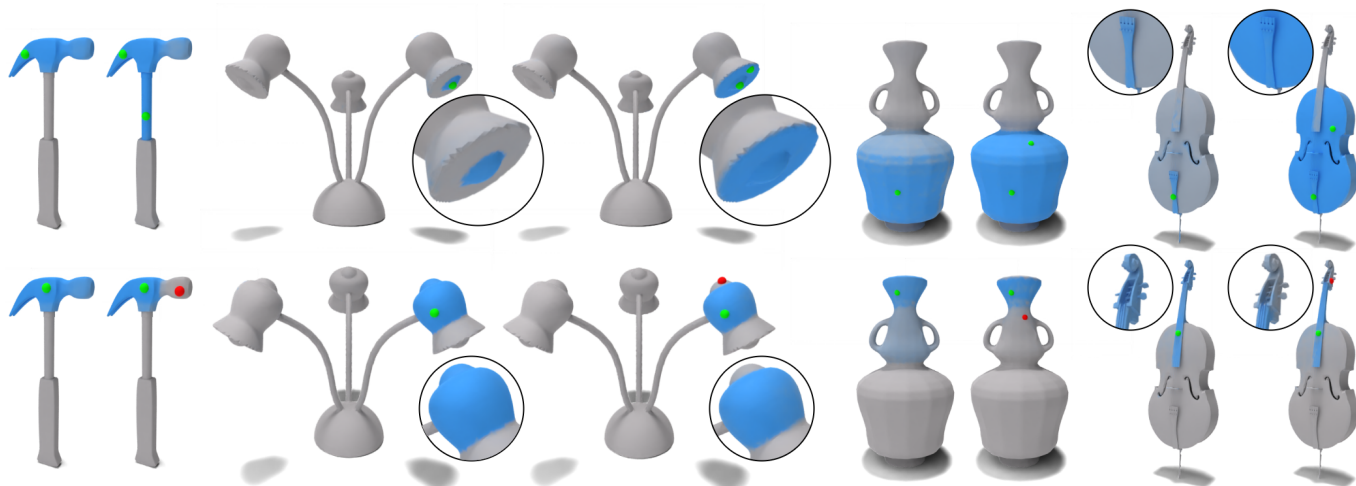


Fig. 6. **Couple of clicks results.** iSeg produces fine-grained segmentations from a couple of clicks (both positive and negative) as input. Each pair of shapes starts with a single positive click (left), which can be further customized using an additional click (right).

to the optimization objective:

$$\mathcal{L}_{dec} = \frac{1}{|\Theta'|} \sum_{\theta' \in \Theta'} \text{CE}(I_p^{\theta'}, I_m^{\theta'}), \quad (7)$$

where CE denotes the binary cross-entropy loss.

To prepare data for our 3D decoder training, we simulate user clicks and generate probability masks from the 2D model [Kirillov et al. 2023]. The data generation process includes 2 phases. First, we pick a subset of the mesh vertices uniformly, where each vertex is regarded as a single positive click. For each selected vertex, we generate random views, feed each one through the 2D foundation model, and get the reference segmentation mask. Then, for each view, we randomly sample another vertex visible within the viewing angle, which is set to be a positive or a negative click, and compute the updated segmentation by the 2D model. According to its type, we require the second click to increase or decrease the previous segmentation mask to obtain rich and diverse training data.

As seen in Fig. 3, the supervision signal is highly inconsistent. The 3D shape and the same clicks are interpreted differently by the 2D model, yielding strong variations in the 2D segmentation masks. Nonetheless, our method reveals a coherent underlying 3D segmentation function out of the noisy 2D measurements. Our decoder utilizes the robust distilled 3D vertex features, applies their interaction with the clicked points, and computes the region probability map directly in 3D. iSeg segmentations are view-consistent *by construction*, improving substantially over its training data. Furthermore, although trained with only 2D supervision, iSeg delineates meaningful regions in 3D that are not entirely visible in a single 2D projection (Fig. 5).

4 EXPERIMENTS

We evaluate iSeg in a variety of aspects. First, we demonstrate the generality and fidelity of our method in Sections 4.1 and 4.2, respectively. Then, in Section 4.3, we showcase properties of iSeg, such as the stability of the segmentation for different clicks and

its inherent 3D consistency. Finally, Section 4.4 presents the strong generalization power of iSeg in terms of the selected point, views of the click, and the number of clicks.

We apply our method to diverse meshes from different sources: COSEG [van Kaick et al. 2011], Turbo Squid [TurboSquid 2021], Thing10K [Zhou and Jacobson 2016], Toys4k [Rehg 2022], ModelNet [Wu et al. 2015], and ShapeNet [Chang et al. 2015]. iSeg is highly robust to the shape properties. It operates on meshes with different numbers of vertices and various geometries, including thin, flat, and high-curvature surfaces.

iSeg is implemented in PyTorch [Paszke et al. 2017] and its training time varies according to the number of mesh vertices. For a mesh with 3000 vertices, the optimization takes about 3 hours on a single Nvidia A40 GPU. Querying the model with input clicks takes about 0.7 seconds on that GPU. In our experiments, we used SAM ViT-H with an image size of 224×224 . To obtain fine-grained segmentations, we utilized the smallest scale mask from SAM for the projected clicked points. Additional details are in the supplementary.

4.1 Generality of iSeg

iSeg is highly versatile and works on a variety of shapes and geometries. It is not limited to any specific shape category nor a pre-defined set of parts and can be applied to meshes from various domains, including humanoids, animals, musical instruments, household objects, and more. Our method is also applicable to shapes with complex geometric structures and is optimized to capture the elements of the given object.

Fig. 2 presents different single-click results. iSeg successfully segments regions with sharp edges, such as the neck of the lamp and the thin spokes of the bike. It also captures accurately the flat surface of the alien’s head and the curved lower part of its leg. Moreover, iSeg can segment small parts of the shape - the bike’s seat and the water bottle, or larger portions, such as the body parts of the camel.

Method	InterObject3D	SAM Baseline	iSeg (ours)
Effectiveness \uparrow	2.54	3.02	4.55

Table 1. **Perceptual user study.** We compare the 3D segmentation effectiveness for different clicked-based interactive methods on a scale of 1 to 5, corresponding to completely ineffective and completely effective segmentation. Our method is considered much more effective than the competitors.

4.2 Fidelity of iSeg

Our method’s training is supervised by segmentation masks generated from SAM [Kirillov et al. 2023] for 2D renderings of the shape. As we show in Figs. 3 and 9, SAM’s masks differ substantially between views. In contrast, iSeg manages to fuse the noisy training examples into a coherent 3D segmentation model that corresponds to the clicked vertices. Examples are presented in Figs. 2 and 6.

iSeg is adapted to the granularity of the given mesh, which enables it to adhere to the user’s clicks and segment the region of the shape related to the user’s inputs. For example, in Fig. 2, for a click on the alien’s middle antenna, the entire antenna and *only that particular antenna* is selected. We see similar behavior for other clicks, such as the one on the lamp’s base and the camel’s neck.

In Fig. 6, we further show the results of iSeg for a couple of clicks. We incorporate either a second positive click that extends the segmented part or a second negative click that retracts the region. For example, with the first click, the fine-grained bulb area of the lamp is segmented. Then, the second positive click enables including the flat surface surrounding the bulb. The negative click, on the other hand, offers the control to reduce and refine the segmentation region. As shown in Fig. 6, the first click on the hammer’s head segments the entire head. The front part can be easily and intuitively removed by a second negative click on it.

Perceptual user study. As far as we can ascertain, there is no dataset with ground-truth annotation for click-based interactive segmentation of 3D shapes. Thus, for quantitative evaluation of our method, we opt to perform a perceptual user study. We used 20 meshes from different categories, such as humanoids, animals, and man-made objects, and included 40 participants in our study.

For each mesh, we showed the 3D segmentation for a clicked point from multiple viewing angles and asked the participants to rate the effectiveness of the result on a scale of 1 to 5. The score 5 refers to a completely effective segmentation, where the entire 3D region corresponding to the clicked point is selected. When part of the 3D region is marked, the segmentation is considered partially effective. The score 1 is defined as a completely ineffective segmentation and refers to no region selection. Examples are presented in Fig. 12.

For comparison, we considered two alternatives, InterObject3D [Kontogianni et al. 2023] and a baseline we constructed based on SAM’s 2D segmentations. InterObject3D is a recent work on interactive segmentation of 3D objects. For the SAM baseline, we rendered the shape and projected the clicked point to 2D from 100 random views, computed SAM’s mask, and re-project the result back to 3D for each visible vertex. Then, we averaged the predictions according to the number of times each vertex was seen. Other interactive segmentation techniques use an implicit 3D representation [Chen



Fig. 7. **Segmentation stability.** The region selected by iSeg remains stable and consistent even when selecting different points within the same region.

et al. 2023b] or perform a different task (object detection) [Zhang et al. 2023], and thus, are not directly comparable to our method.

Fig. 15 presents several example questions from our study, demonstrating the comparison between the alternative segmentation techniques, and Tab. 1 summarizes the effectiveness score averaged over all the meshes and participants in the study. Fig. 13 further compares our method with the SAM baseline. As seen in the figures and reflected by the table, the participants rate the effectiveness of iSeg much higher than the other methods, indicating its fidelity to the clicked point by the user.

Applications. iSeg computes contiguous and localized shape partitions. These segmentations enable geometric local editing of the mesh, as demonstrated in Fig. 11. Further details are provided in the supplementary material.

4.3 Properties of iSeg

Stability. A desired property of a click-based segmentation model is to be stable. That is, the results should be similar for nearby clicks that relate to the same shape part. This property implies that the model is robust to the exact click location and alleviates the need for precision from the user. Fig. 7 demonstrates the stability of our method. As the figure shows, iSeg consistently selects the handle part of the hammer for different clicks along the handle.

We evaluate the stability property quantitatively by comparing the segmentation prediction for neighboring vertices. Given a clicked point, we compute the Intersection over Union (IoU) for its resulting mask and the mask for clicking each of its one-ring neighbors. We use 7 meshes with 100 random clicks from each mesh. For comparison, we utilize the SAM baseline, as described in Sec. 4.2. The average IoU for iSeg is 0.8 compared to 0.7 for the SAM baseline. SAM’s masks originate from 2D views of the shape. These predictions do not segment occluded regions of the shape and are less smooth in 3D. In contrast, our method operates directly in 3D and exhibits better stability than the SAM baseline.

3D consistency. Different from SAM [Kirillov et al. 2023], our method operates natively in 3D. iSeg predicts the segmentation probability at the vertex level, or in other words, our result lives on the 3D surface of the mesh. Thus, it is 3D-consistent *by construction*. In Fig. 9, we compare our segmentation projected to 2D with SAM’s result for the projected shape views. Since SAM operates on each view independently, it yields inconsistent predictions. By contrast, in our case, any 2D projection originates from the same 3D segmentation and thus, our method is consistent across all views.

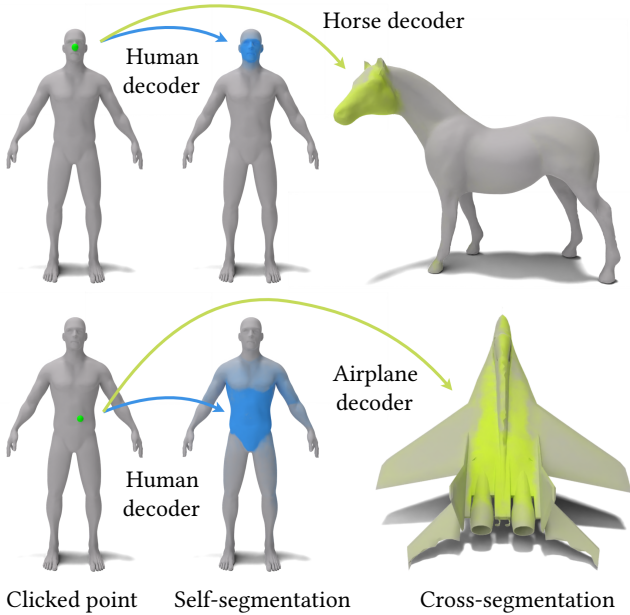


Fig. 8. **Cross-domain segmentation.** iSeg optimizes a condition-agnostic feature field, which is capable of transferring between shapes. The feature vector of a point click of one mesh (left) is used to segment the same shape (middle) as well as *another* shape from a *different* domain (right).

Generic feature information. Our mesh feature field is distilled directly from SAM’s encoder and is independent of the user’s point clicks for segmentation. Thus, although iSeg is optimized per mesh, the semantic feature representation is shared across shapes. We demonstrate this property by cross-domain segmentation. In this experiment, we use the point encoded features from one shape and predict region probability with a *different* shape’s decoder. Fig. 8 shows examples. The transferable features enable the creation of cross-domain shape analogies, such as how the belly of a human corresponds to the “belly” of an airplane.

4.4 Generalization Capabilities

Unseen vertices. Our method exhibits strong generalization power. First, we emphasize that we train just on a small fraction of 3% of the mesh vertices. Still, iSeg is successfully applied to other vertices unseen during training and properly respects the clicked points, as shown in Figs. 2 and 6 and discussed in Sec. 4.2. We note that all the results shown in the paper are for test vertices.

Unseen views. Although iSeg was trained with 2D supervision only, its predictions are 3D in nature. Fig. 5 exemplifies this phenomenon. A click on the back side of the backrest segments the front side as well. Such supervision does not exist for our model’s training, since the clicked vertex cannot be seen from the front side. Similarly, two clicks at opposite sides of the backrest segment the entire part, although they cannot be seen together from *any single 2D view*. This result suggests that iSeg learned 3D-consistent semantic vertex information, enabling it to generalize beyond its 2D supervision.

Unseen number of clicks. For resource efficient training, we trained iSeg on up to two clicks: single click, second positive click,

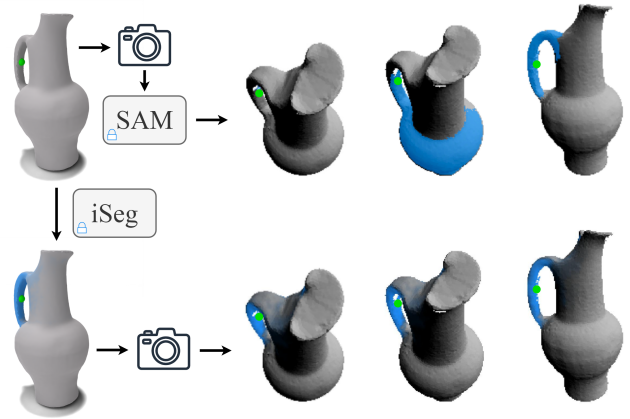


Fig. 9. **Segmentation consistency.** SAM is highly sensitive to the viewing angle. It may generate substantially different masks for similar views, which are inconsistent in 3D. In contrast, iSeg is 3D consistent by construction.

and second negative click. Nonetheless, our model offers customized segmentation with more than two clicks, as demonstrated in Fig. 10. We attribute this capability to the interactive attention mechanism. The interactive attention layer seemed to learn the representation of a positive and a negative click, and how to attend to each click for a meaningful multi-click segmentation.

5 CONCLUSION

In this work, we presented iSeg, a technique for interactively generating fine-grained tailored segmentations of 3D meshes. We opt to lift features from a powerful pre-trained 2D segmentation model onto a 3D mesh, which can be used to create customized user-specified segmentations. Our mesh feature field is general and can be used for additional tasks such as cross-segmentation across shapes of different categories (e.g. Fig. 8). Key to our method is an interactive attention mechanism that learns a unified representation for a varied number of positive or negative point clicks. Our 3D-consistent segmentation enables selecting points across occluding surfaces and segmenting meaningful regions directly in 3D (e.g. Fig. 5).

In the future, we are interested in exploring additional applications of mesh feature fields beyond segmentation. We have demonstrated they may be used for cross-domain segmentation, and there may be other exciting applications, such as key-point correspondence, texture transfer, and more.

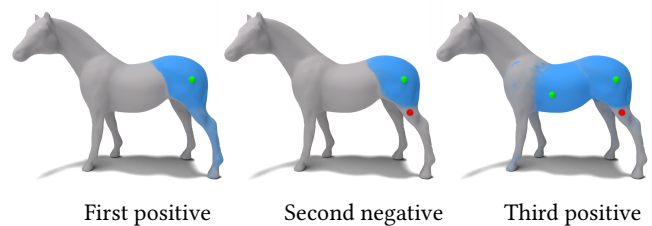


Fig. 10. **Customized segmentations.** iSeg is capable of creating customized segmentations specified by several input clicks.

REFERENCES

- Ahmed Abdelreheem, Abdelrahman Eldesokey, Maks Ovsjanikov, and Peter Wonka. 2023a. Zero-Shot 3D Shape Correspondence. *SIGGRAPH Asia 2023 Conference Papers* (2023).
- Ahmed Abdelreheem, Ivan Skorokhodov, Maks Ovsjanikov, and Peter Wonka. 2023b. SATR: Zero-Shot Semantic Segmentation of 3D Shapes. In *Proceedings of the IEEE/CVF International Conference on Computer Vision (ICCV)*.
- I. Armeni, A. Sax, A. R. Zamir, and S. Savarese. 2017. Joint 2D-3D-Semantic Data for Indoor Scene Understanding. *ArXiv e-prints* (Feb. 2017). arXiv:1702.01105 [cs.CV]
- Yuri Y Boykov and M-P Jolly. 2001. Interactive graph cuts for optimal boundary & region segmentation of objects in ND images. In *Proceedings eighth IEEE international conference on computer vision. ICCV 2001*, Vol. 1. IEEE, 105–112.
- Jiazhong Cen, Zanwei Zhou, Jiemin Fang, Chen Yang, Wei Shen, Lingxi Xie, Dongsheng Jiang, Xiaopeng Zhang, and Qi Tian. 2023. Segment Anything in 3D with NeRFs. arXiv:2304.12308 [cs.CV]
- Angel X Chang, Thomas Funkhouser, Leonidas Guibas, Pat Hanrahan, Qixing Huang, Zimo Li, Silvio Savarese, Manolis Savva, Shuran Song, Hao Su, et al. 2015. Shapenet: An information-rich 3d model repository. *arXiv preprint arXiv:1512.03012* (2015).
- Xiaokang Chen, Jiaxiang Tang, Diwen Wan, Jingbo Wang, and Gang Zeng. 2023b. Interactive Segment Anything NeRF with Feature Imitation. arXiv:2305.16233 [cs.CV]
- Zhimin Chen, Longlong Jing, Yingwei Li, and Bing Li. 2023a. Bridging the Domain Gap: Self-Supervised 3D Scene Understanding with Foundation Models. arXiv:2305.08776 [cs.CV]
- Zhiqin Chen, Kangxue Yin, Matthew Fisher, Siddhartha Chaudhuri, and Hao Zhang. 2019. Bae-net: Branched autoencoder for shape co-segmentation. In *Proceedings of the IEEE/CVF International Conference on Computer Vision*. 8490–8499.
- Nicu D Cornea, Deborah Silver, and Patrick Min. 2007. Curve-skeleton properties, applications, and algorithms. *IEEE Transactions on visualization and computer graphics* 13, 3 (2007), 530.
- Dale Decatur, Itai Lang, Kfir Aberman, and Rana Hanocka. 2023a. 3D Paintbrush: Local Stylization of 3D Shapes with Cascaded Score Distillation. *arXiv preprint arXiv:2311.09571* (2023).
- Dale Decatur, Itai Lang, and Rana Hanocka. 2023b. 3D Highlighter: Localizing Regions on 3D Shapes via Text Descriptions. In *Proceedings of the IEEE/CVF Conference on Computer Vision and Pattern Recognition (CVPR)*. 20930–20939.
- Boyang Deng, Kyle Genova, Soroosh Yazdani, Sofien Bouaziz, Geoffrey Hinton, and Andrea Tagliasacchi. 2020. Cvxnet: Learnable convex decomposition. In *Proceedings of the IEEE/CVF Conference on Computer Vision and Pattern Recognition*. 31–44.
- Tamal K Dey and Wulue Zhao. 2004. Approximating the medial axis from the Voronoi diagram with a convergence guarantee. *Algorithmica* 38, 1 (2004), 179–200.
- Rahul Goel, Dhawal Sirikonda, Saurabh Saini, and PJ Narayanan. 2023a. Interactive Segmentation of Radiance Fields. arXiv:2212.13545 [cs.CV]
- Rahul Goel, Dhawal Sirikonda, Saurabh Saini, and P. J. Narayanan. 2023b. Interactive Segmentation of Radiance Fields. In *Proceedings of the IEEE/CVF Conference on Computer Vision and Pattern Recognition (CVPR)*. 4201–4211.
- Huy Ha and Shuran Song. 2022. Semantic Abstraction: Open-World 3D Scene Understanding from 2D Vision-Language Models. In *Proceedings of the 2022 Conference on Robot Learning*.
- Rana Hanocka, Amir Hertz, Noa Fish, Raja Giryes, Shachar Fleishman, and Daniel Cohen-Or. 2019. MeshCNN: A Network with an Edge. *ACM Transactions on Graphics (TOG)* 38, 4 (2019), 90:1–90:12.
- Donald D Hoffman and Whitman A Richards. 1984. Parts of recognition. *Cognition* 18, 1-3 (1984), 65–96.
- Yining Hong, Yilun Du, Chunru Lin, Josh Tenenbaum, and Chuhan Gan. 2022. 3D Concept Grounding on Neural Fields. In *Annual Conference on Neural Information Processing Systems*.
- Shi-Min Hu, Zheng-Ning Liu, Meng-Hao Guo, Junxiong Cai, Jiahui Huang, Tai-Jiang Mu, and Ralph R. Martin. 2022. Subdivision-based Mesh Convolution Networks. *ACM Trans. Graph.* 41, 3 (2022), 25:1–25:16. <https://doi.org/10.1145/3506694>
- Justin Kerr, Chung Min Kim, Ken Goldberg, Angjoo Kanazawa, and Matthew Tancik. 2023. LERF: Language Embedded Radiance Fields. arXiv:2303.09553 [cs.CV]
- Alexander Kirillov, Eric Mintun, Nikhila Ravi, Hanzi Mao, Chloe Rolland, Laura Gustafson, Tete Xiao, Spencer Whitehead, Alexander C. Berg, Wan-Yen Lo, Piotr Dollar, and Ross Girshick. 2023. Segment Anything. In *Proceedings of the IEEE/CVF International Conference on Computer Vision (ICCV)*. 4015–4026.
- Sosuke Kobayashi, Eiichi Matsumoto, and Vincent Sitzmann. 2022. Decomposing NeRF for Editing via Feature Field Distillation. *arXiv* (2022).
- Theodora Kontogianni, Ekin Celikkan, Siyu Tang, and Konrad Schindler. 2023. Interactive Object Segmentation in 3D Point Clouds. arXiv:2204.07183 [cs.CV]
- Abhijit Kundu, Xiaoqi Yin, Alireza Fathi, David Ross, Brian Brewington, Thomas Funkhouser, and Caroline Pantofaru. 2020. Virtual Multi-view Fusion for 3D Semantic Segmentation. *arXiv e-prints*, Article arXiv:2007.13138 (July 2020), arXiv:2007.13138 pages. <https://doi.org/10.48550/arXiv.2007.13138> arXiv:2007.13138 [cs.CV]
- Alon Lahav and Ayellet Tal. 2020. Meshwalker: Deep mesh understanding by random walks. *ACM Transactions on Graphics (TOG)* 39, 6 (2020), 1–13.
- Anat Levin, Dani Lischinski, and Yair Weiss. 2007. A closed-form solution to natural image matting. *IEEE transactions on pattern analysis and machine intelligence* 30, 2 (2007), 228–242.
- Jyh-Ming Lien and Nancy M Amato. 2007. Approximate convex decomposition of polyhedra. In *Proceedings of the 2007 ACM symposium on Solid and physical modeling*. 121–131.
- Francesco Milano, Antonio Loquercio, Antoni Rosinol, Davide Scaramuzza, and Luca Carlone. 2020. Primal-dual mesh convolutional neural networks. *Advances in Neural Information Processing Systems* 33 (2020), 952–963.
- Ben Mildenhall, Pratul P. Srinivasan, Matthew Tancik, Jonathan T. Barron, Ravi Ramamoorthi, and Ren Ng. 2020. NeRF: Representing Scenes as Neural Radiance Fields for View Synthesis. *arXiv e-prints*, Article arXiv:2003.08934 (March 2020), arXiv:2003.08934 pages. <https://doi.org/10.48550/arXiv.2003.08934> arXiv:2003.08934 [cs.CV]
- Fausto Milletari, Nassir Navab, and Seyed-Ahmad Ahmadi. 2016. V-Net: Fully Convolutional Neural Networks for Volumetric Medical Image Segmentation. arXiv:1606.04797 [cs.CV]
- Adam Paszke, Sam Gross, Soumith Chintala, Gregory Chanan, Edward Yang, Zachary DeVito, Zeming Lin, Alban Desmaison, Luca Antiga, and Adam Lerer. 2017. Automatic differentiation in PyTorch. In *NIPS-W*.
- Charles R. Qi, Hao Su, Kaichun Mo, and Leonidas J. Guibas. 2017. PointNet: Deep Learning on Point Sets for 3D Classification and Segmentation. arXiv:1612.00593 [cs.CV]
- James Matthew Rehg. 2022. Toys4K 3D Object Dataset. <https://github.com/rehglab/lowshot-shapebias/tree/main/toys4k>.
- Carsten Rother, Vladimir Kolmogorov, and Andrew Blake. 2004. GrabCut - Interactive Foreground Extraction using Iterated Graph Cuts. *ACM Transactions on Graphics (SIGGRAPH)* (August 2004). <https://www.microsoft.com/en-us/research/publication/grabcut-interactive-foreground-extraction-using-iterated-graph-cuts/>
- Ariel Shamir. 2008. A survey on mesh segmentation techniques. *Computer graphics forum* 27, 6 (2008), 1539–1556.
- Nicholas Sharp, Souhaib Attaiki, Keenan Crane, and Maks Ovsjanikov. 2022. Diffusion-net: Discretization agnostic learning on surfaces. *ACM Transactions on Graphics (TOG)* 41, 3 (2022), 1–16.
- Mario Sormann, Christopher Zach, and Konrad Karner. 2006. Graph Cut Based Multiple View Segmentation for 3D Reconstruction. In *Third International Symposium on 3D Data Processing, Visualization, and Transmission (3DPVT'06)*. 1085–1092. <https://doi.org/10.1109/3DPVT.2006.70>
- Weimei Sun, Andrea Tagliasacchi, Boyang Deng, Sara Sabour, Soroosh Yazdani, Geoffrey E Hinton, and Kwang Moo Yi. 2021. Canonical Capsules: Self-Supervised Capsules in Canonical Pose. In *Advances in Neural Information Processing Systems*, M. Ranzato, A. Beygelzimer, Y. Dauphin, P.S. Liang, and J. Wortman Vaughan (Eds.), Vol. 34. Curran Associates, Inc., 24993–25005. <https://proceedings.neurips.cc/paper/2021/file/d1ee59e20ad01cedc15f5118a7626099-Paper.pdf>
- TurboSquid. 2021. TurboSquid 3D Model Repository. <https://www.turbosquid.com/>.
- Oliver van Kaick, Andrea Tagliasacchi, Oana Sidi, Hao Zhang, Daniel Cohen-Or, Lior Wolf, and Ghassan Hamarneh. 2011. Prior knowledge for part correspondence. *Computer Graphics Forum* 30, 2 (2011), 553–562. <https://doi.org/10.1111/j.1467-8659.2011.01893.x>
- Ashish Vaswani, Noam Shazeer, Niki Parmar, Jakob Uszkoreit, Llion Jones, Aidan N Gomez, Łukasz Kaiser, and Illia Polosukhin. 2017. Attention Is All You Need. *Advances in neural information processing systems* 30 (2017).
- Zhirong Wu, Shuran Song, Aditya Khosla, Fisher Yu, Linguang Zhang, Xiaoou Tang, and Jianxiong Xiao. 2015. 3d shapenets: A deep representation for volumetric shapes. In *Proceedings of the IEEE conference on computer vision and pattern recognition*. 1912–1920.
- Yunhan Yang, Xiaoyang Wu, Tong He, Hengshuang Zhao, and Xihui Liu. 2023. SAM3D: Segment Anything in 3D Scenes. *arXiv e-prints*, Article arXiv:2306.03908 (June 2023), arXiv:2306.03908 pages. <https://doi.org/10.48550/arXiv.2306.03908> arXiv:2306.03908 [cs.CV]
- Jianglong Ye, Naiyan Wang, and Xiaolong Wang. 2023. FeatureNeRF: Learning Generalizable NeRFs by Distilling Foundation Models. arXiv:2303.12786 [cs.CV]
- Li Yi, Hao Su, Xingwen Guo, and Leonidas J Guibas. 2017. Syncspecnn: Synchronized spectral cnn for 3d shape segmentation. In *Proceedings of the IEEE conference on computer vision and pattern recognition*. 2282–2290.
- Yuanwen Yue, Sabarinath Mahadevan, Jonas Schult, Francis Engelmann, Bastian Leibe, Konrad Schindler, and Theodora Kontogianni. 2023. AGILE3D: Attention Guided Interactive Multi-object 3D Segmentation. arXiv:2306.00977 [cs.CV]
- Dingyuan Zhang, Dingkan Liang, Hongcheng Yang, Zhikang Zou, Xiaoqing Ye, Zhe Liu, and Xiang Bai. 2023. SAM3D: Zero-Shot 3D Object Detection via Segment Anything Model. *arXiv e-prints*, Article arXiv:2306.02245 (June 2023), arXiv:2306.02245 pages. <https://doi.org/10.48550/arXiv.2306.02245> arXiv:2306.02245 [cs.CV]
- Renrui Zhang, Liuhui Wang, Yu Qiao, Peng Gao, and Hongsheng Li. 2022. Learning 3D Representations from 2D Pre-trained Models via Image-to-Point Masked Autoencoders. arXiv:2212.06785 [cs.CV]

- Qian Zheng, Zhuming Hao, Hui Huang, Kai Xu, Hao Zhang, Daniel Cohen-Or, and Baoquan Chen. 2015. Skeleton-Intrinsic Symmetrization of Shapes. *Computer Graphics Forum* 34, 2 (2015), 275–286.
- Qingnan Zhou and Alec Jacobson. 2016. Thingi10K: A Dataset of 10,000 3D-Printing Models. *arXiv preprint arXiv:1605.04797* (2016).
- Chenyang Zhu, Kai Xu, Siddhartha Chaudhuri, Li Yi, Leonidas J Guibas, and Hao Zhang. 2020. AdaCoSeg: Adaptive Shape Co-Segmentation with Group Consistency Loss. In *Proceedings of the IEEE/CVF Conference on Computer Vision and Pattern Recognition*. 8543–8552.

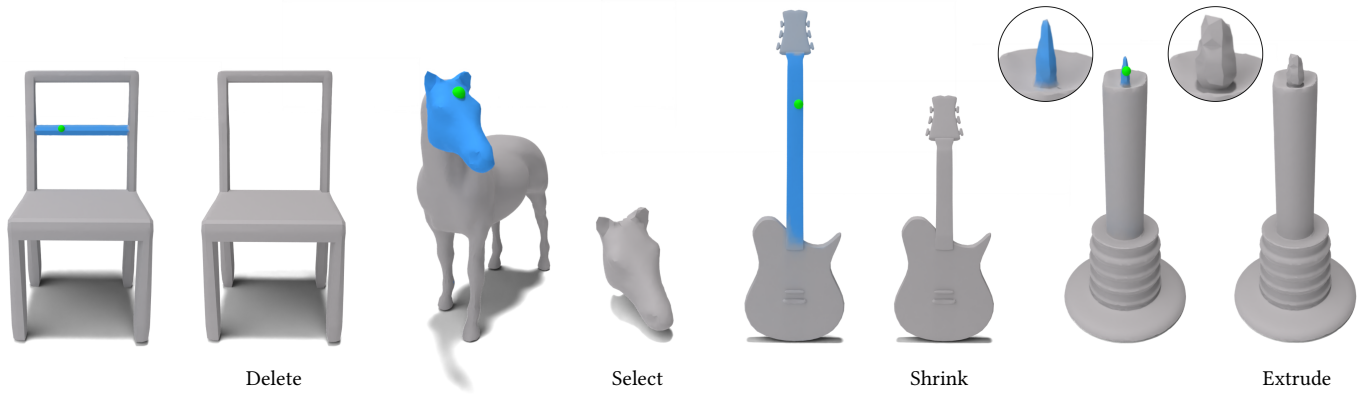


Fig. 11. **Local geometric edits.** Our localized and contiguous segmentations enable various shape edits, such as deleting or selecting the segmented region, shrinking it, or extruding it along the surface normal.

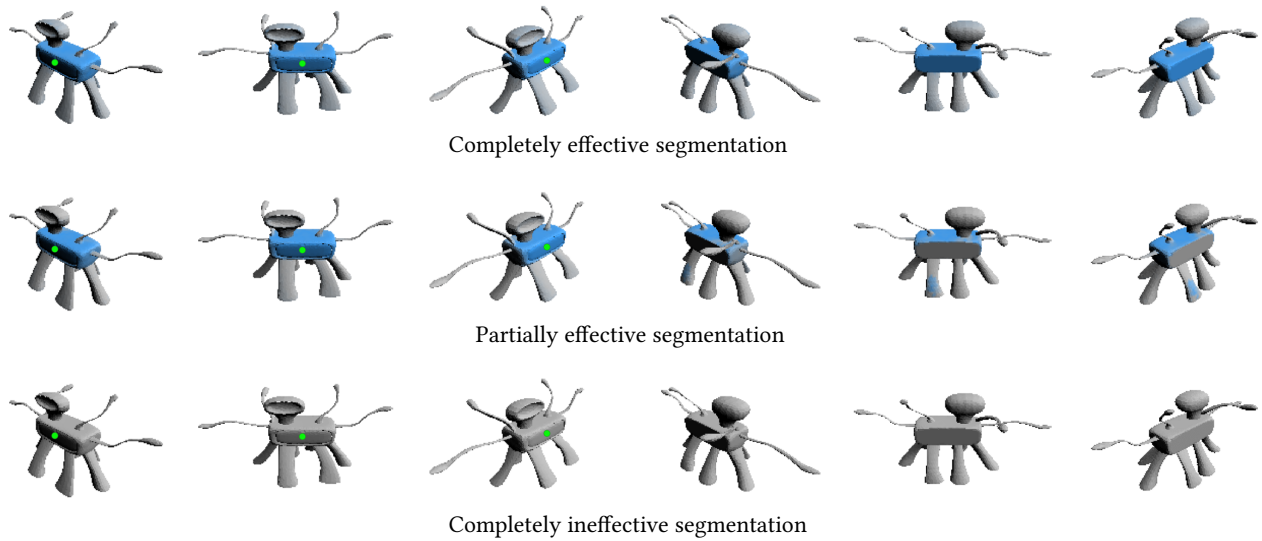


Fig. 12. **Segmentation effectiveness.** We visualize results with a varying level of effectiveness, as presented in our perceptual user study. The segmentations from top to bottom rows are considered completely effective, partially effective, and completely ineffective, respectively.

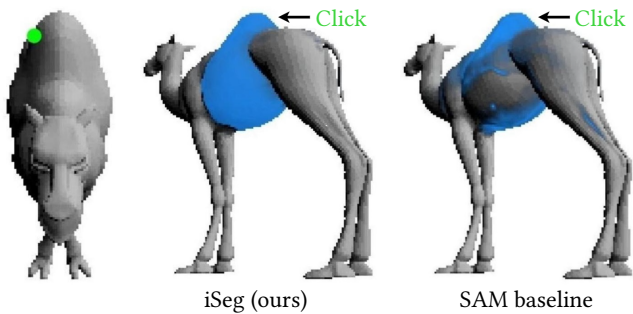


Fig. 13. **The power of iSeg for occluded point click.** When the point click (green dot in the leftmost image) is occluded, iSeg can produce an effective 3D segmentation (highlighted in blue), whereas the SAM baseline is unable to do so.

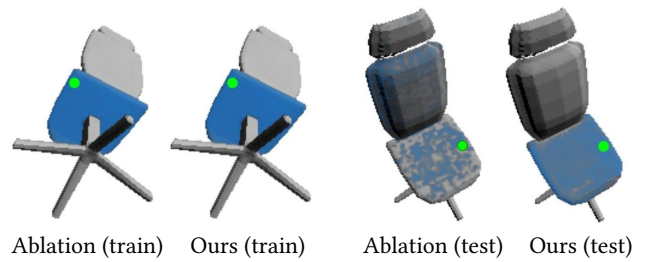


Fig. 14. **Ablation test.** We compare an iSeg model from separate training of the encoder and decoder with an ablation model from joint training of both components. Our proposed separate training scheme results in better generalization for test vertices.

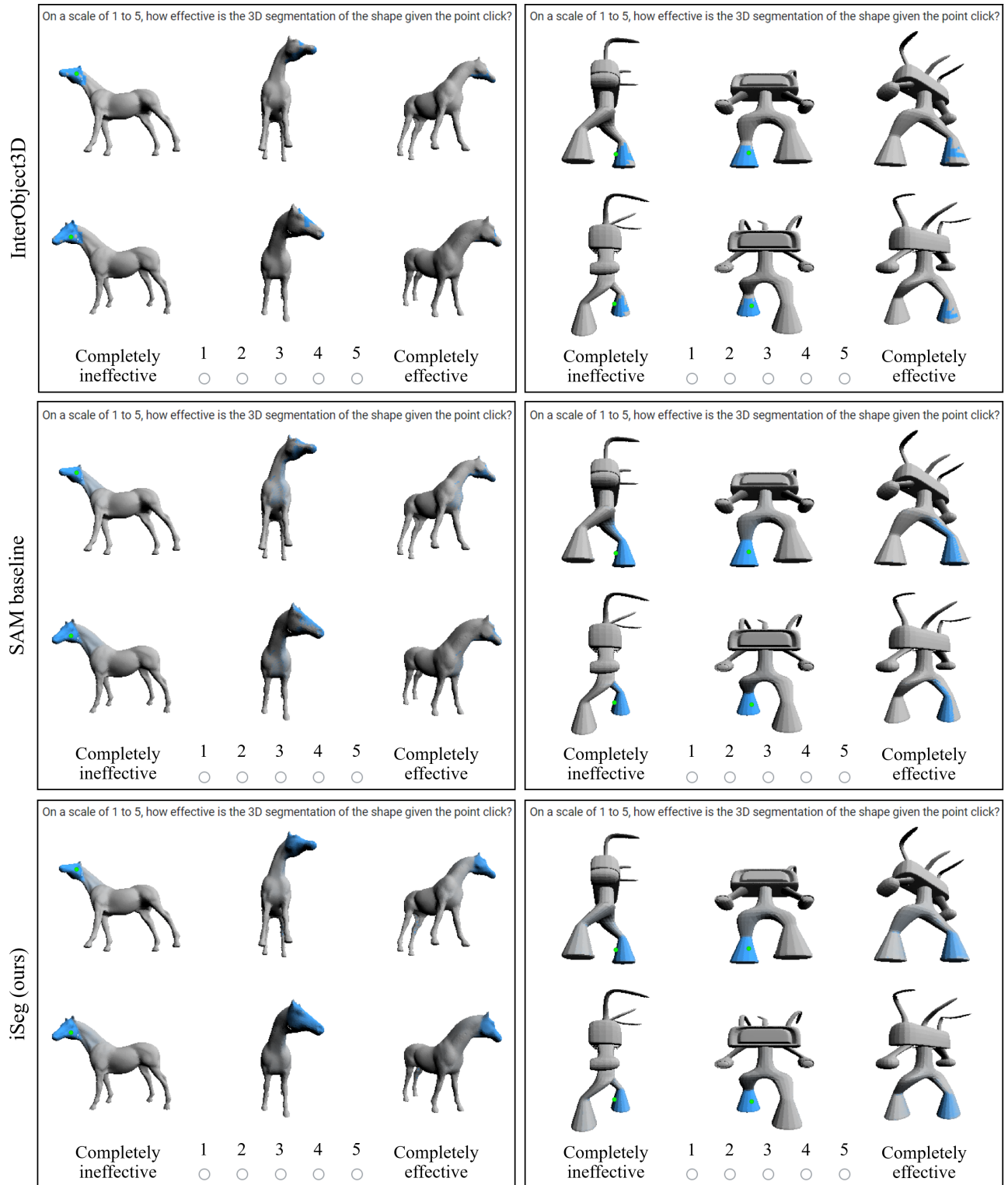


Fig. 15. **Perceptual study example questions.** For each mesh, we ask the participants to rate the effectiveness of the segmentation for the compared methods, where they are unaware of which method is used. The other techniques are perceived as partially effective, as they do not mark the entire 3D region corresponding to the clicked point. In contrast, iSeg selects complete regions in a 3D-consistent fashion and is considered highly effective.

iSeg: Interactive 3D Segmentation via Interactive Attention

Supplementary Material

The following sections provide more information regarding our interactive segmentation method. Appendix A shows additional results and experiments we conducted with iSeg. Appendix B discusses our perceptual user study. In appendix C, we detail the results of an ablation test. Finally, in appendix D, we elaborate on our implementation details for the encoder and decoder networks and the comparison settings to previous work.

A ADDITIONAL RESULTS

View generalization, cross-segmentation, and stability. Figs. 16, 17 and 20 present additional examples of the view generalization of iSeg, its cross-domain segmentation ability, and the stability of the selected region. In Fig. 16, we show that iSeg segments the whole body of the guitar, even though its back side is occluded from the click on the front. Moreover, the second click on the back side of the guitar’s bridge cannot be seen together in any 2D view with the first click. Nevertheless, our method selects the complete 3D regions of the bridge and body.

Fig. 17 shows that the semantic information of iSeg’s features is shared between different shapes, and enables cross-domain segmentation of similar parts. Interestingly, for the click on the front right leg of the camel, the front right leg of the chair was mostly selected.

In Fig. 20, we present the segmentation stability of iSeg. For a couple of clicks, the user can select the entire trailer box or only its side with various locations for the positive clicks or positive and negative clicks, respectively.

Granularity. Fig. 18 exemplifies an additional property of our method: segmentation granularity. When segmenting the leg for an intricate shape like the human body, the user can control whether to exclude the foot, the lower shin part, or the upper part of the calf muscle by simply clicking the negative point at different locations along the leg.

Separability. We analyze iSeg’s segmentation prediction by plotting the histogram of probability values for all the shape vertices for different clicks. Results are presented in Fig. 21. We observe that the histogram contains two populations: vertices with high segmentation probability, which correspond to the region for the clicked point, and the rest of the vertices with low probability. To further demonstrate the separability of the model’s predictions, we use the Otsu threshold and binarize the probabilities. As shown in the figure, the region before and after thresholding remains almost the same, indicating that the segmented part can be easily separated from the shape.

Applications. In Fig. 11 in the main body, we show how our method’s results are used for local shape editing. iSeg selection corresponds to a contiguous region of an entire part of the shape. Thus, the segmented part can be easily manipulated. As the figure demonstrates, the entire bar of the chair is removed, only the head of the horse can be selected, the neck of the guitar is shortened, and a small local region of the candle’s flame is enlarged.

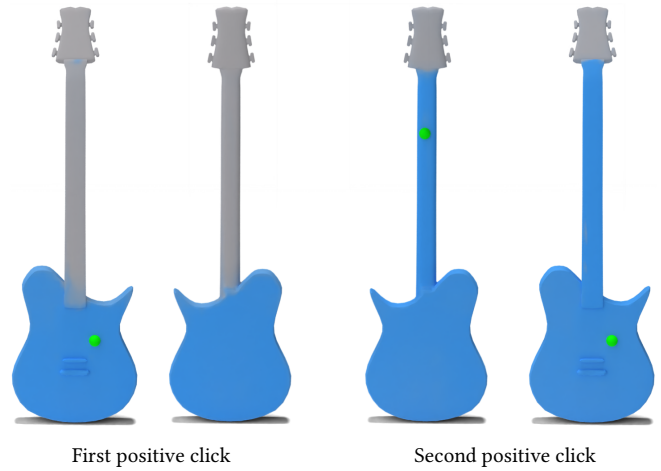


Fig. 16. **View generalization.** Although our method was trained only with 2D supervision, it produces 3D segmentations for regions and clicks at opposite sides of the shape that cannot be seen together in 2D.

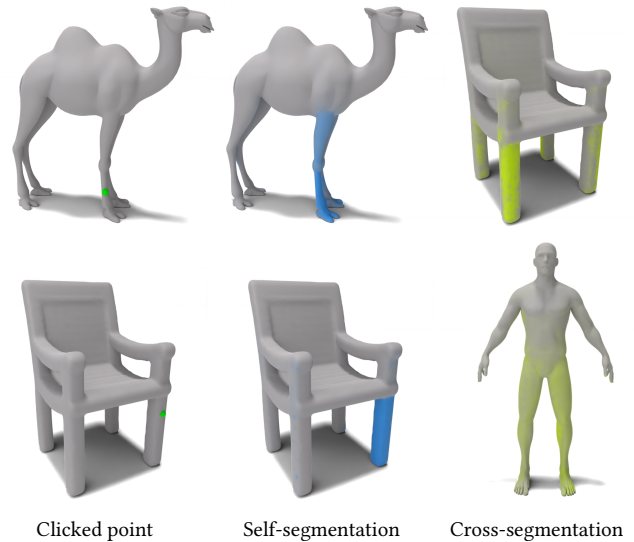


Fig. 17. **Cross-domain segmentation.** iSeg learned features generalize across domains. The feature vector of a clicked point results in the selection of a similar semantic region for the shape itself and a shape from a different domain.

Limitation. Our method may not follow the symmetry of the mesh exactly, as exemplified in Fig. 19. For a click on the goat’s head, the segmented regions from the sides of the head differ somewhat from each other. The other face side is occluded from the clicked point, thus iSeg is not trained to segment those regions the same and does not produce a symmetric mask for both sides.

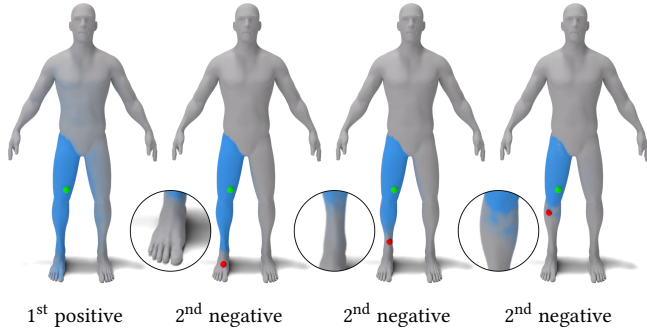


Fig. 18. **Segmentation granularity.** iSeg offers control over the segmented region according to the location of the clicked point.

B PERCEPTUAL USER STUDY

In Fig. 12 in the main paper, we show segmentation results with different levels of effectiveness, as exemplified in our perceptual user study (discussed in Sec. 4.2). In the presented example, the point click is on the cubic region of an alien shape, and the segmentation result is visualized from different viewing angles, part of which the clicked point is occluded.

The example in the top row is considered *completely effective* with a score of 5 since the whole cubic region of the alien is segmented and no other region is selected. The result in the middle row is considered *partially effective*, since not the whole cubic region is segmented (the back of the box is not selected), and a region other than the box is marked (part of the back leg). In the last row, the segmentation is considered *completely ineffective* with a score of 1, since no region from the shape is selected (there is no blue color). The participants in our study were shown the segmentation results of each of the compared methods for each mesh and rated them according to the scoring explanation elaborated here.

The results from our perceptual study, reported in Tab. 1 in the paper, suggest that the segmented regions by iSeg are considered highly effective, compared to the partially effective segmentations by SAM baseline. This finding is consistent with the 2D nature of SAM. It is challenging to generate meaningful segmentation for occluded parts in 3D. For example, in Fig. 13 in the paper, the user’s point click is on one side of the camel’s hump. For a viewing angle where the click is not visible, the SAM baseline can only segment the hump partially. In contrast, iSeg fully segments the hump, even though the point click is occluded from the presented viewing angle. Due to iSeg’s 3D consistency, it can combine shape information from different viewing angles to produce an effective segmentation that is meaningful in 3D.

C ABLATION TEST

We performed an ablation experiment of training the encoder and decoder together, rather than separately, as proposed in our method. We optimized the parameters of both the encoder and decoder (including the parameters of the interactive attention layer) together considering the loss of both the encoder and decoder. The loss function in the ablation test was:

$$\mathcal{L} = w\mathcal{L}_{enc} + \mathcal{L}_{dec}, \quad (8)$$

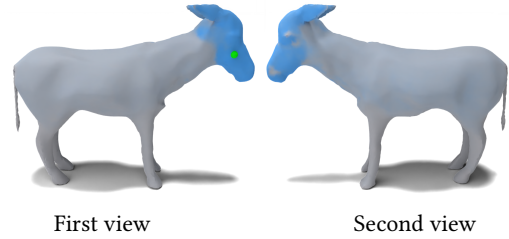


Fig. 19. **Limitation.** iSeg may not produce a symmetric segmentation result for a symmetric shape. In this case, the segmented region of one side of the shape is different than the other.

where $w = 5$ is the weight of the encoder loss. The definitions of \mathcal{L}_{enc} and \mathcal{L}_{dec} are the same as in the main paper: \mathcal{L}_{enc} is the l_2 loss between the projected mesh feature field and SAM’s 2D embedding for the rendered shape image, and \mathcal{L}_{dec} is the binary cross-entropy loss between the rasterized iSeg probability prediction and the reference 2D segmentation mask from SAM. We use a similar view generation scheme as in the main paper to train the ablation model.

We found that the ablation model and the original model proposed in the main paper perform equally well for the training vertices, as shown on the left side of Fig. 14 in the main paper. However, the ablation model suffers from over-fitting due to the high flexibility of the network when training the encoder and the decoder simultaneously, making it less powerful on the test vertices, as shown on the right side of Fig. 14. iSeg generalizes better when trained for the same number of epochs as the ablation model.

D IMPLEMENTATION DETAILS

Encoder. We use the vertex coordinates of the mesh and apply positional encoding of size 515, which is the input to our encoder. The encoder is implemented as a multi-layer perceptron (mlp) of 6 layers, with 256 neurons per layer. Each layer except the last includes ReLU activation and layer normalization. After the last layer, we apply hyperbolic tangent activation without normalization. The encoder’s output is a per-vertex feature vector of size 256.

Decoder. The interactive attention module contains linear layers of size 256×256 for W^Q , W_{pos}^K , W_{neg}^K , W_{pos}^V , and W_{neg}^V . The output of this layer of size 256 is concatenated to the per-vertex encoded feature vector of size 256 to a total size of 512. Then, a 16-layer mlp operates on the concatenated feature vector. The mlp has the first layer of size 512, 14 layers of size 256, and the last layer of size 2. Each layer except the last includes ReLU activation and layer normalization. After the last layer, we apply a Softmax operation without normalization.

Compared method. As mentioned in the main body (Sec. 4.2), we compared the effectiveness of our method with the recent interactive segmentation work InterObject3D [Kontogianni et al. 2023]. We adopted their publicly available pretrained model¹ and added channels for point clicks, as instructed in their paper. For our experiments, we set the volume length for the point click to 0.05.

¹<https://github.com/theodorakontogianni/InterObject3D/tree/main>

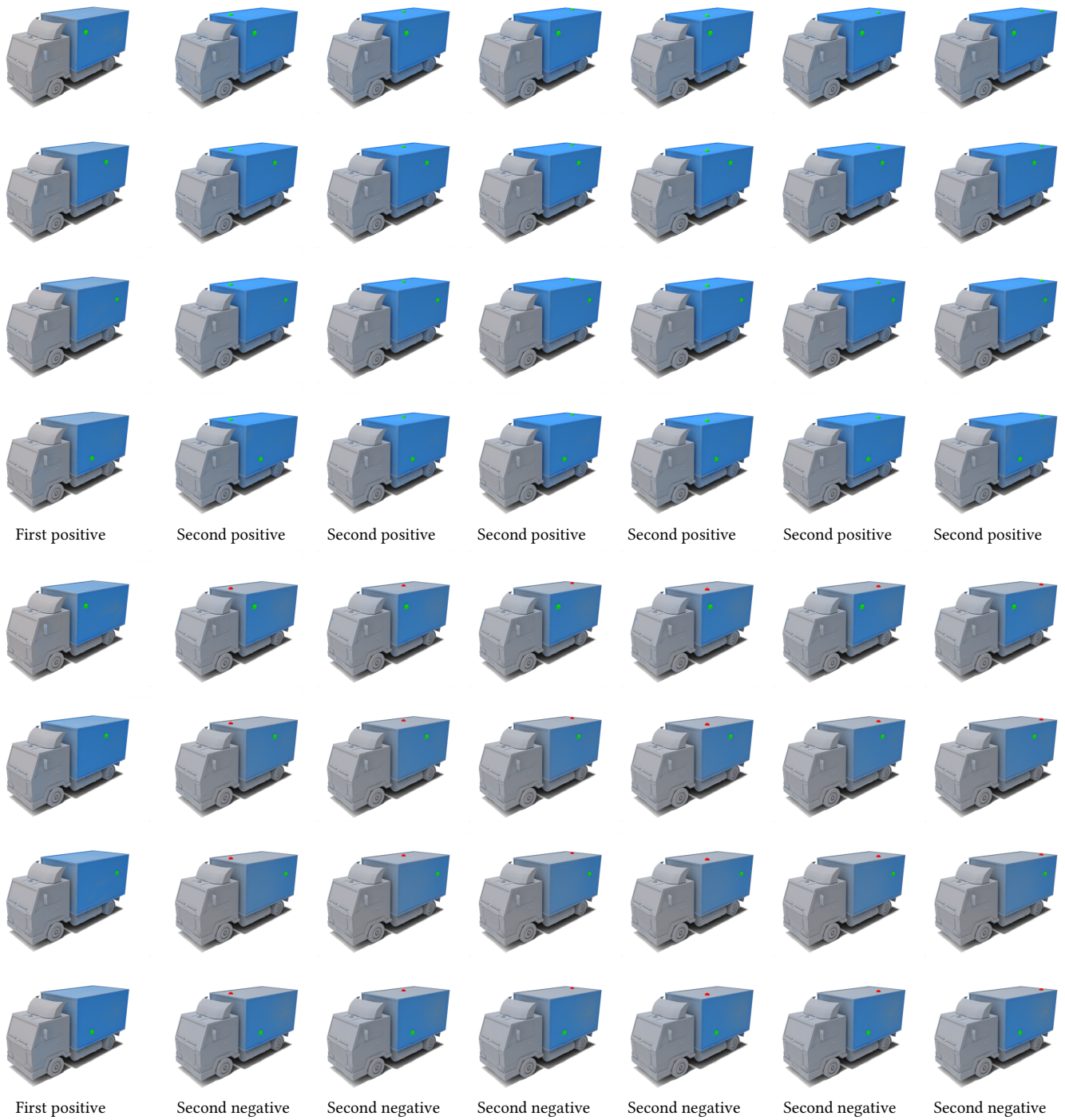


Fig. 20. **Segmentation stability for a couple of clicks.** The segmented region remains similar for positive and negative clicks with varying click locations over the semantic shape region.

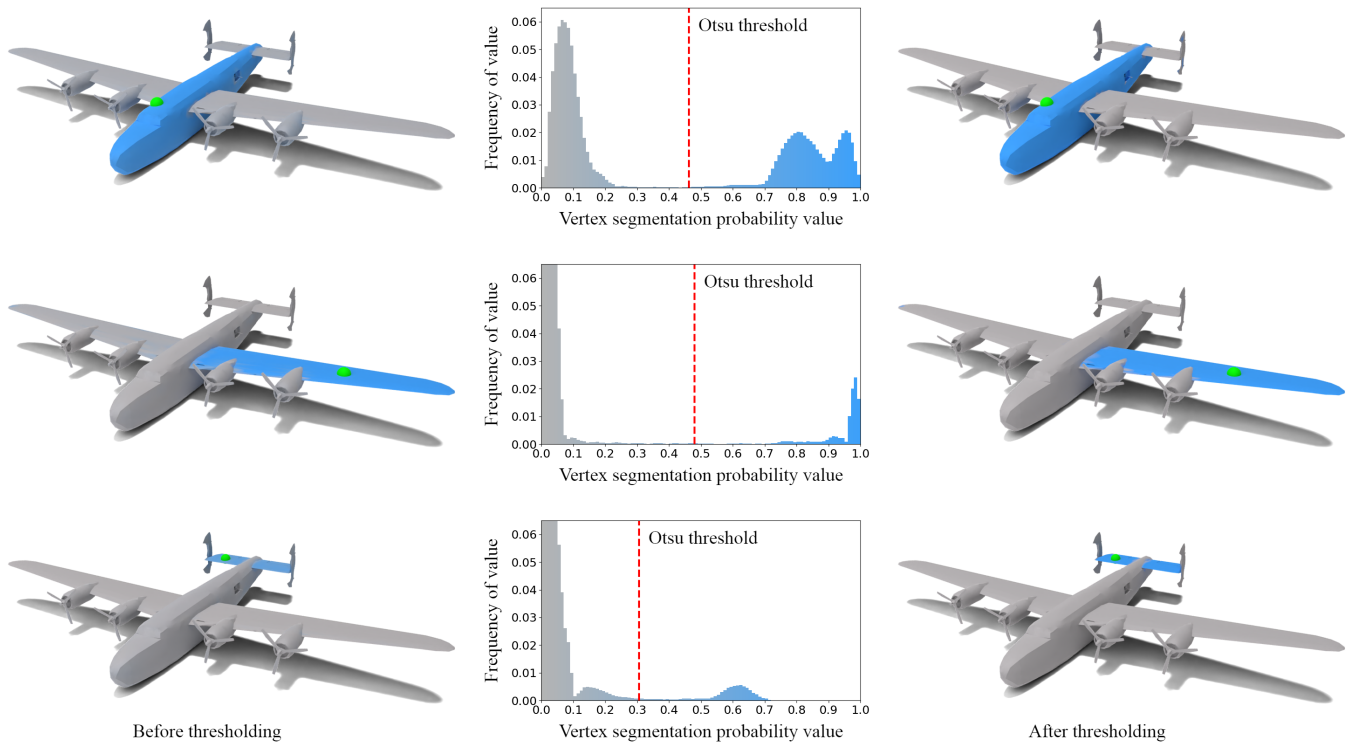


Fig. 21. **Segmentation separability.** The per-vertex segmentation probability can be separated distinctively into low and high value populations, which enables the hard selection of the segmented part by simple thresholding.